Geomechanics and Engineering, *Vol. 19, No. 6 (2019) 499-511*
DOI: https://doi.org/10.12989/gae.2019.19.6.499

Rock burst criteria of deep residual coal pillars in an underground coal mine: a case study

Pengqi Qiu[a], Jun Wang*, Jianguo Ning[b], Xuesheng Liu[c], Shanchao Hu[d] and Qingheng Gu[e]

State Key Laboratory of Mining Disaster Prevention and Control Co-founded by Shandong Province and the Ministry of Science and Technology, Shandong University of Science and Technology, 579 Qianwangang Road, Qingdao, China

(Received March 29, 2019, Revised November 10, 2019, Accepted November 17, 2019)

Abstract. The reliability of reinforced concrete structures is frequently compromised by the deterioration caused by reinforcement corrosion. Evaluating the effect caused by reinforcement corrosion on structural behaviour of corrosion damaged concrete structures is essential for effective and reliable infrastructure management. In lifecycle management of corrosion affected reinforced concrete structures, it is difficult to correctly assess the lifecycle performance due to the uncertainties associated with structural resistance deterioration. This paper presents a stochastic deterioration modelling approach to evaluate the performance deterioration of corroded concrete structures during their service life. The flexural strength deterioration is analytically predicted on the basis of bond strength evolution caused by reinforcement corrosion, which is examined by the experimental and field data available. An assessment criterion is defined to evaluate the flexural strength deterioration for the time-dependent reliability analysis. The results from the worked examples show that the proposed approach is capable of evaluating the structural reliability of corrosion damaged concrete structures.

Keywords: rock burst; criteria; back-analyses; residual coal pillars; numerical analysis

1. Introduction

In China, large-scale pillars are often needed to maintain the stability of the mining roadway and ensure the ventilation and transportation demand of the working face in the mining of deep coal resources. Currently, certain old underground mines in China, especially in eastern and northeast China, are often require retreat mining of coal pillars to improve coal resource recovery rates, and extend the mine life. Underground coal extraction practices indicated that longwall panel retreat creates stress concentrations around coal pillars, and may cause the already highly- stressed pillars to burst. For example, during the mining of residual pillars in the 1410 working face of the Huafeng Coal Mine, Shandong Province, rock burst was induced by the presence of a strong stress zone, resulting in casualties and equipment damage. Mazaira *et al.* (2015) noted that to minimize the impact of rock burst, the first step is to predict the zones that are prone to suffering rock burst. Therefore, there is a need to establish a suitable criterion for the prediction of zones with rock burst potential.

Researchers have proposed many hazard criteria (indices) of rock burst from the perspectives of strength, stiffness, fracture damage, mutation, fracturing and energy. Brady *et al.* (2006) obtained the stiffness of pillars and surrounding rocks by numerical analysis, and analyzed the danger of rock burst. On the basis of summarizing a large number of engineering cases, Hoek *et al.* (2010) determined the influence of σ_v/σ_c on the failure mode of brittle rock mass. They proposed that the ratio of the maximum principal stress to the uniaxial compressive strength of brittle hard rock (σ_v/σ_c) be used as a classification index of the failure mode of brittle rock mass; and established a classification method of rock burst grade. Mitri (1999) proposed the burst potential index (BPI) to evaluate rock burst and analyzed the possible location of strain-type rock burst in Canadian pillars. In view of the risk assessment of coal mine rock burst, Zhu *et al.* (2018) based on distribution characteristics of mining stress, defined the ratio of abutment stress to uniaxial compressive strength of coal (σ_{max}/σ_c) as the impact risk index, and corresponding criteria of rock burst stress was established for different mining faces. Other scholars(Wang *et al.* 2018a, Liu *et al.* 2018, Wang *et al.* 2018b, Liu *et al.* 2019, Fan *et al.* 2019) established different energy indexes of rock burst, which were aimed at the actual situation of rock burst in mines under the specific engineering conditions in China. Their results lay the foundation for the prediction and prevention of rock burst. However, there is no criterion for evaluating rock burst in multi pillar mining. To solve the problems of

*Corresponding author, Professor
E-mail: wangjunsdkjd@126.com
[a]Ph.D. Student
E-mail: qiupengqi@163.com
[b]Ph.D.
E-mail: njglxh@126.com
[c]Ph.D.
E-mail: xuesheng1134@163.com
[d]Ph.D.
E-mail: 329964724@qq.com
[e]Student
E-mail: 15610451523@163.com

ISSN: 2005-307X (Print), 2092-6219 (Online)

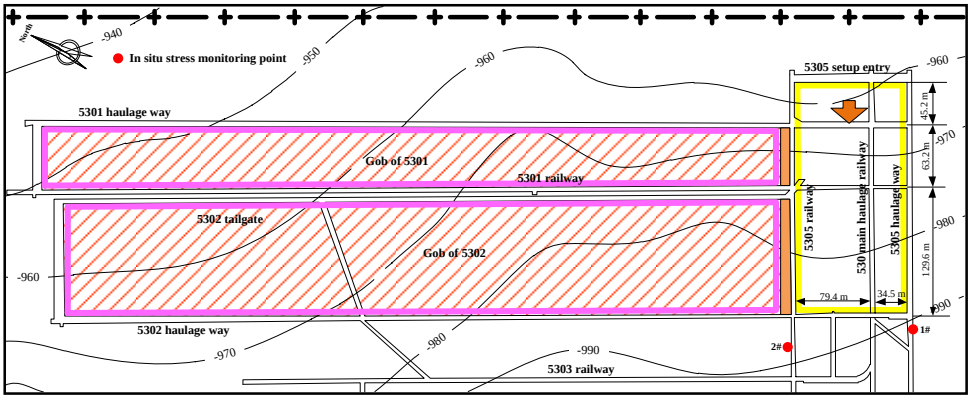

Fig. 1 Layout of panels 5301, 5302 and 5305

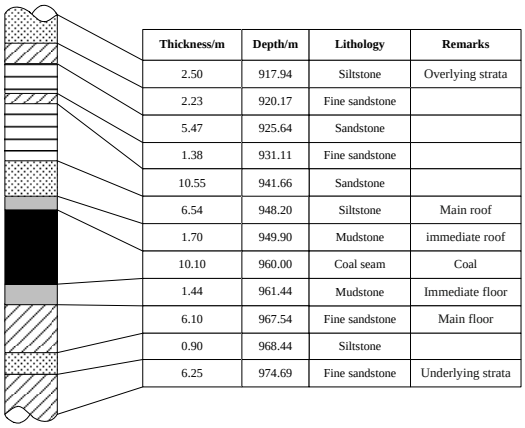

Thickness/m	Depth/m	Lithology	Remarks
2.50	917.94	Siltstone	Overlying strata
2.23	920.17	Fine sandstone	
5.47	925.64	Sandstone	
1.38	931.11	Fine sandstone	
10.55	941.66	Sandstone	
6.54	948.20	Siltstone	Main roof
1.70	949.90	Mudstone	immediate roof
10.10	960.00	Coal seam	Coal
1.44	961.44	Mudstone	Immediate floor
6.10	967.54	Fine sandstone	Main floor
0.90	968.44	Siltstone	
6.25	974.69	Fine sandstone	Underlying strata

Fig. 2 Generalized stratigraphic column of the study site

Table 1 Layout of panels 5301, 5302 and 5305

Measuring stations	Maximum principal stress(σ_1)			Intermediate principal stress(σ_2)			Minimum principal stress(σ_3)			Vertical stress(σ_Z)
	Value /MPa	Azimuth angle/°	Dip angle/°	Value /MPa	Azimuth angle/°	Dip angle/°	Value /MPa	Azimuth angle/°	Dip angle/°	Value/ MPa
1	28.41	S89.3°E	12.5	23.18	N42.3°E	71.5	22.54	S2.3°E	-13.3	24.72
2	28.66	S87.0°E	18.1	24.53	N65.7°E	70.6	23.25	S5.1°E	6.6	24.91

Table 2 Generalized stratigraphic column of the study site

Coal burst proneness index	D_T/ms	K_E	W_{ET}	R_C/MPa
Schematic drawing of calculation	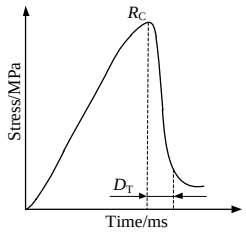	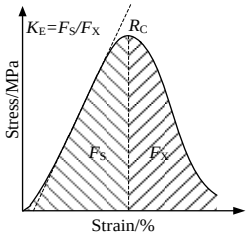	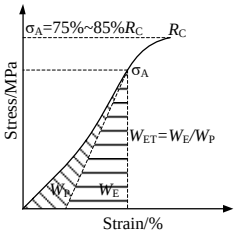	
Test method	Uniaxial compression test			
Strong burst	≤50	≥5.0	≥5.0	≥14
Weak burst	50-500	1.5-5	2-5	7-14
None burst	>500	<1.5	<2	<7

these mines (the mining of deep residual coal pillars is threatened by rock burst), it is necessary to establish evaluation criteria for rock burst in multi pillar mining faces.

In this paper, the characteristics of a specific working face with deep residual pillars are selected. Taking panel 5305 of the Shandong Xinhe Coal Mine as a research example, combined with field cases and monitoring data,

the evolution characteristics of the advance vertical stress during mining of the working face are studied by numerical simulation. Combining the numerical results with mine rock burst events, certain existing evaluation indexes of rock burst risk have been revised, and evaluation indexes of rock burst risk suitable for the current research background have been obtained. The research findings can provide certain references for the safe mining of deep coal pillars.

2. Engineering background

2.1 Overview of the engineering geological characteristics

The selected panel, panel 5305 of the Xinhe Coal Mine, is located in Jining City, Shandong Province. Panel 5305 is mining the no. 3 coal seam. The coal seam is buried at a depth of approximately 976.8-1020.0 m. The average thickness of the no. 3 coal seam is approximately 10.1 m, ith a dip angle of 6º, as shown in Fig. 1. Panel 5305 has a length of 257 m along the strike and 126 m along the dip.

As shown in Fig. 1, the northwest areas 5301 and 5302 contain gob, and the southeast part is solid coal. The northeast parts of the area adjacent to panel 5305 contain boundary pillars of adjacent mines, and the southwest parts contain the 530 main roadways, 5305 main return airways and 5305 main haulage roadways. The most notable characteristic of panel 5305 is that the panel is divided into six pillar areas of different sizes by the mining roadways (the 5301 haulage gateway, 5302 tailgate and 530 gathering main roadway), servicing the premining face (panels 5301 and 5302). The 5301 haulage gateway, 5302 tailgate and 5305 setup entry are parallel, while the 530 gathering main roadway is vertical to the 5305 setup entry, as shown in Fig 1. Fig. 2 depicts the generalized stratigraphic column of the study site, which is constructed based on core logging data. As shown in Fig. 2, the immediate roof, which is approximately 29.8 m thick, is composed of sandstone, siltstone, fine sandstone and mudstone.

The rock strata above the coal seam are, in ascending order, sandy mudstone (1.7 m), fine siltstone (6.54 m), gritstone (10.55 m) and siltstone (1.38 m), while the rock strata below the coal seam are, in descending order, mudstone (1.44 m), siltstone (6.1 m) and siltstone (0.9 m). The generalized stratigraphy column is shown in Fig. 2.

2.2 In situ stress field

In situ stress is one of the most fundamental factors controlling the mode of stress-induced fracturing, particularly when the underground mining depth increases (Zhao *et al.* 2018, Liu *et al.* 2019). For this reason, a good understanding of the natural stress state influencing the rock mass behavior of the underground coal excavation is necessary. In this study, the stress-relief method was used to estimate the in situ stress with two measurements, as shown in Fig. 1. Table 1 summarizes the measurement results. The characteristics of the in situ stress field can be considered as follows:

(1) The maximum principal stress is approximately 28.41-28.66 MPa, the azimuth is approximately between S89.3°E and S87.0°E, and the inclination is approximately 12.5-18.1º;

(2) The vertical stress is approximately 24.72-24.91 MPa, and its value is similar to the vertical stress of 23 MPa calculated according to the thickness and bulk density of the overlying strata (the depth of the roadway is 964 m, while the average bulk density of the overlying strata is 2.3 t/m^3);

(3) The angle between the maximum principal stress and the horizontal plane is less than 20°, indicating that the maximum principal stress in the Xinhe Mine is nearly horizontal. The stress field in this area is primarily horizontal. The ratio of the maximum horizontal stress σ_H to the vertical stress σ_V is approximately 1.15, which means that the lateral pressure coefficient in this area is 1.15.

The results of the in situ stress test show that the in situ stress of the Xinhe Mine is high, which has a greater impact on roadway stability.

Table 3 CBL test results

CBL index	D_T/ms	K_E	W_{ET}	R_C/MPa	Classification
No.3 coal seam	84-362	1.409-1.846	7.331-13.034	17.878-20.977	**Strong burst**

2.3 Coal burst risk

Because rock burst is a sudden release of strain energy stored in the coal seam, the coal's tendency to burst depends on its capacity to store and release elastic strain energy. The coal's tendency to burst, which is also called the coal burst proneness, can be illustrated by the elastic strain energy index (W_{ET}), bursting energy index (K_E) and dynamic failure duration (D_T). W_{ET} focuses on the capacity of the coal to store elastic strain energy, which is the ratio of the elastic strain energy accumulated in the specimen to the dissipative strain energy. The larger the value of W_{ET}, the less the coal can dissipate energy via plastic deformation and the greater the susceptibility to burst. K_E is defined as the ratio of deformation energy stored prepeak and postpeak dissipated energy and is considered the energy accumulated and subsequently dissipated. These two indexes can be used to evaluate the ability of energy accumulation and energy release. Laboratory tests and theoretical findings have shown that if the coal is weak, the failure duration will last longer, and energy will be released slowly. However, if the coal is hard, strong and brittle, the failure duration is shorter, and energy will be released suddenly and the rock burst potential will be great. Therefore, these three indexes were used to evaluate the coal's tendency to burst. The classification and calculation method of the coal burst proneness are shown in Table 2, according to Chinese standards (GB/T 25217.2-2010, 2010).

The coal burst proneness indexes were measured using coal samples obtained from the no. 3 coal seam of the Xinhe Coal Mine. Table 3 lists the test results for each coal burst proneness index: W_{ET} was approximately 7.331-13.034, K_E was approximately 1.409-1.846, R_C was approximately 17.878-20.977 and D_T was approximately 84-362. All these indexes indicated that the coal had the capacity to store energy and release energy in a short time and was therefore liable to burst.

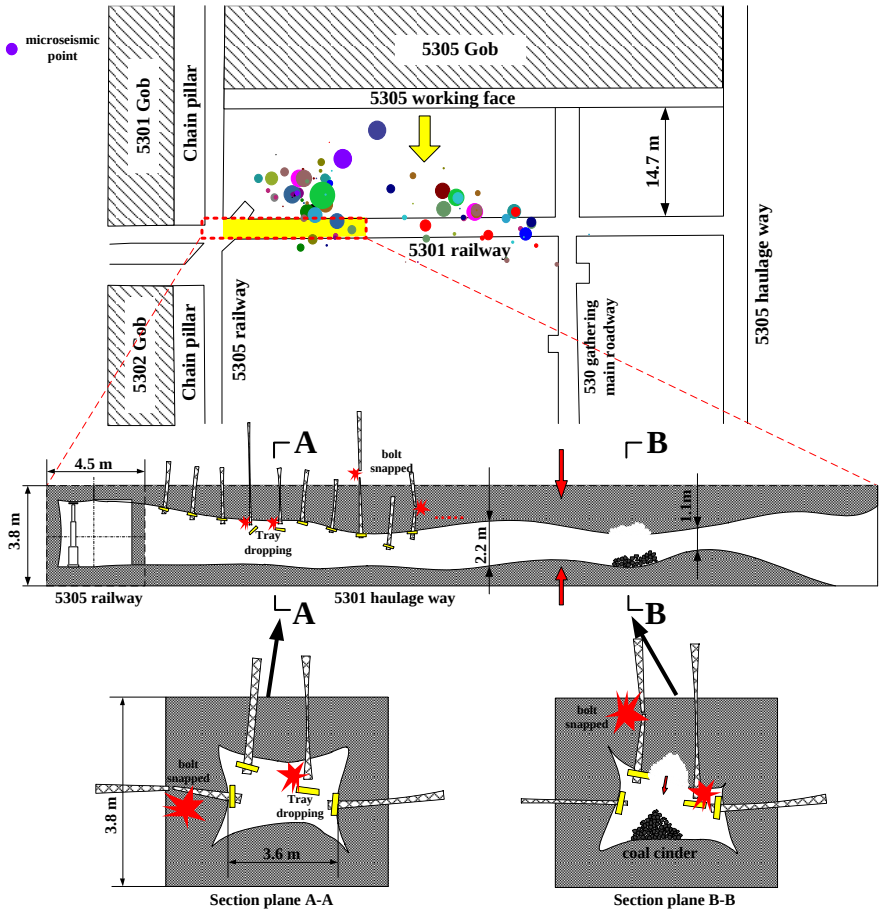

Fig. 3 The location of the “6.16” event and the characteristics of the damaged roadway

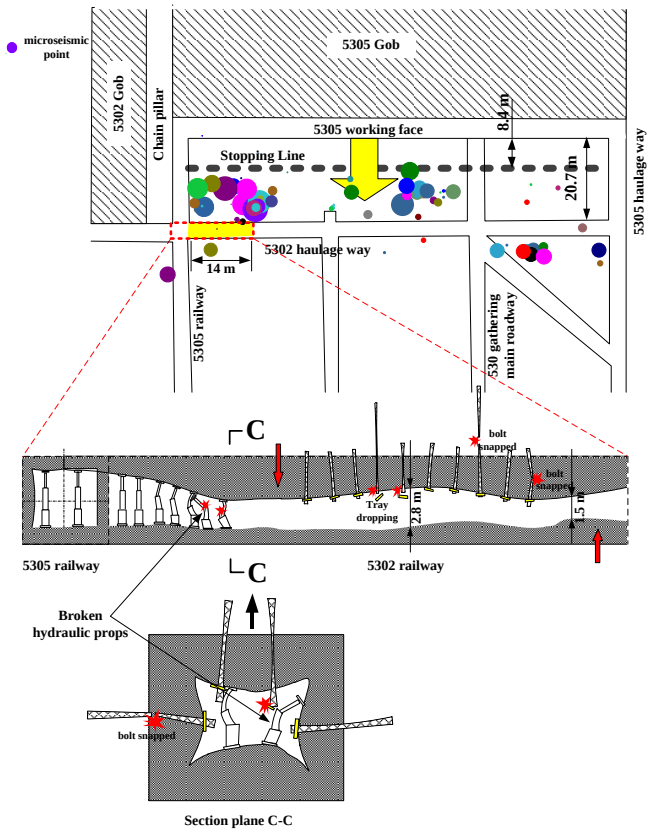

Fig. 4 The location of the “7.24” event and the characteristics of the damaged roadway

2.4 Case Study

2.4.1 The "6.16" event

On June 16, 2018, at 11:05 am, when the 5305 working face had advanced 126 m from the setup room, rock burst occurred 14.7 m ahead of the longwall face in the 5301 railway, as shown in Fig. 3. When the "6.16" event occurred, a solid block of coal was thrown into roadway, and the roof-to-floor/rib-to-rib convergence ranged from 1.5-2.0 m. At the most severe deformation location, the dimensions of the roadway changed from 3.8x4.5 m to 2.6x3.6 m, and 12 cables and 13 bolts were destroyed. Field geological investigations showed that there were no faults, dykes or sandstone channels surrounding the damaged roadway. Therefore, geological structures did not contribute to the occurrence of the "6.16" event. Considering the field conditions, the 5301 railways were not used for air return or coal transportation, and certain destressing techniques were applied to mitigate the rock burst.

2.4.2 The "7.24" event

On July 24, 2018, at 19:47 am, as the longwall face advanced 234.8 m, a small rock burst event occurred in the 5302 haulage roadways adjacent to the 5305 tailgate railways, as shown in Fig. 4. At the same time, microseismic monitoring found that on July 24, 2018, the daily microseismic source rate and energy release were very high, and microseismic events with a total energy release of 86291 J were mainly concentrated in the failure zone. Field investigations showed that after the occurrence of rock burst, the 5302 haulage roadway with a length of 14 m suffered a large deformation, and the contraction ratio was up to 50-80%. In addition, the support material was seriously damaged as 13 props were destroyed by distortion, while at least 10 cables and 15 bolts were broken.

3. The 5305 panel model and simulation setup

3.1 Numerical simulation model

3.1.1 Numerical model

In this study, a general numerical model, using the finite-difference software FLAC3D, was built to investigate the stress distribution induced by longwall mining activities in detail. The general numerical model included three panels: panel 5301, panel 5302 and panel 5305. As shown in Fig. 5, the dimensions of the general model were 580 m×370 m×142.5 m. The model was divided into 1168830 zones, which were determined based on model sensitivity analysis. As shown in Fig. 5, a vertical stress of 21.5 MPa was applied at the top model boundary to simulate an overburden pressure by assuming that the overlying unit weight is 0.025 MN/m^3, and a gravity force was applied. The horizontal displacements of the four vertical planes of the model were restricted in the normal direction, and the vertical displacement at the base of the model was set to zero. According to the test results of the in situ stress in the mining area, the in situ stresses were applied in the form of initial stress with the horizontal-to-vertical stress ratio set to 1.15 in the x- and y-directions.

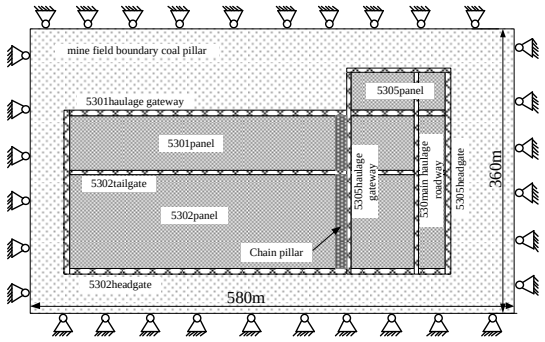

Fig. 5 Coal seam plan of the numerical model

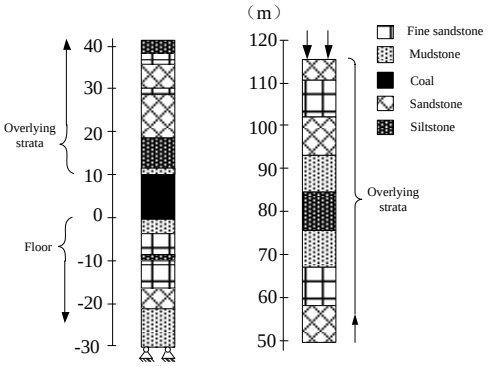

Fig. 6 Geological histogram of the numerical model

Table 4 Rock stratum properties used in the numerical model

Rock strata	Thickness	Density (kg·m^{-3})	Bulk modulus (GPa)	Shear modulus (GPa)	Friction angle (°)	Cohesion (MPa)	Tensile strength (MPa)
Overlying strata	20.00	2500	4.21	3.52	30	1.5	0.52
Fine sandstone	2.50	2700	7.17	6.63	35	2.0	0.77
Sandstone	2.23	2650	6.53	5.63	33	1.6	0.59
Siltstone	5.47	2550	4.97	3.94	32	1.2	0.43
Fine sandstone	1.38	2650	6.53	5.63	33	1.6	0.59
Sandstone	10.55	2550	4.97	3.94	32	1.2	0.43
Siltstone	6.54	2680	4.97	3.94	32	1.2	0.43
Mudstone	1.7	1800	3.17	2.45	31	1.1	0.39
Coal seam	10.10	1400	1.00	0.46	30	1.0	0.035
Mudstone	1.44	1800	3.17	2.45	31	1.1	0.39
Fine sandstone	6.10	2650	6.53	5.63	33	1.6	0.59
Siltstone	0.90	2700	7.17	6.63	35	2.0	0.77
Fine sandstone	6.25	2650	6.53	5.63	33	1.6	0.59
Underlying strata	13.81	2500	4.21	3.52	30	1.5	0.52

3.1.2 Mechanical parameters

An essential step in the numerical model is determination of the rock mass mechanical properties, such as the strength properties and rock mass modulus. In the past, numerous rock mass classification systems have been

Table 5 Strain-softening parameters of the coal seam mechanical properties

Cohesion			Friction		
Original value (MPa)	Softening rate (%)	Residual value (MPa)	Original value (deg.)	Softening rate (%)	Residual value (MPa)
1.0	5	0.1	30	0.5	24

Table 6 Materials parameters for the double-yield model

Parameters	Density(kg/m^3)	Bulk modulus(GPa)	Shear modulus(GPa)	Friction (°)	Dilation (°)
Value	1000	8.87	6.73	22	7

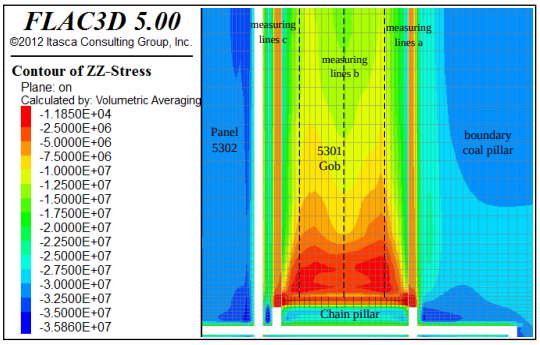

(a)

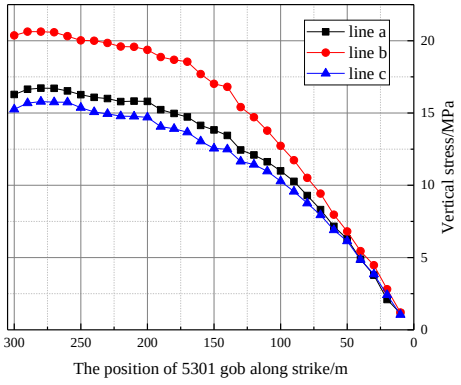

(b)

Fig. 7 Vertical stress of the 5301 gob. (a) Vertical stress contours of the 5301 gob and (b) Vertical stress contours of the three measuring lines

proposed and used, such as the Q system, RQD, the rock mass rating (RMR) method, and the geological strength index (GSI) method to evaluate and classify rock mass. In previous studies, a reduction factor, which was used to scale the intact strength value to the field value, was introduced. Mohammad noted that the rock uniaxial compressive strength (UCS) is on average 0.284 times the intact UCS value. Cai *et al.* (2016) also suggested that for most coal measure lithologies, the elastic modulus, cohesion and tensile can be estimated at 0.1–0.25 of the laboratory test results. These correlations have gained wide acceptance among researchers (Wang *et al.* 2018; Shang *et al.* 2019;). However, there are few guidelines for the determination of the reduction factor. In the current study, the final properties of the coal and rock mass for the model are shown in Table 4.

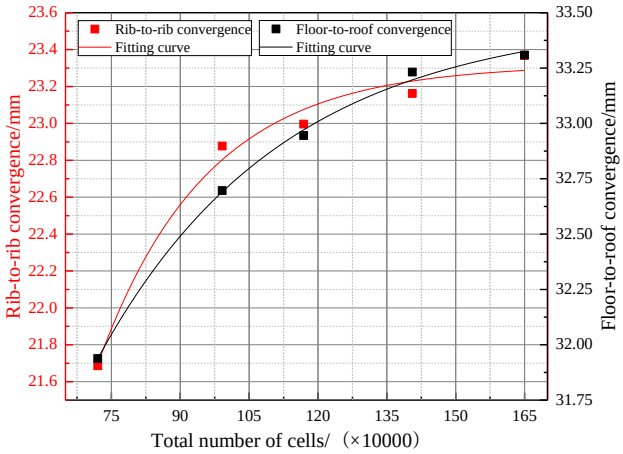

Fig. 8 The convergence of the roadway with different mesh densities

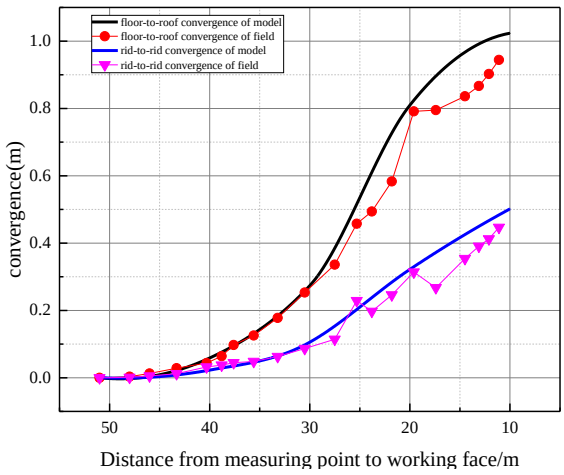

Fig. 9 Comparison diagram of field monitoring convergence and numerical simulation convergence

3.1.3 The constitutive model

Based on past experiences in simulating coal and rocks, in this study, strain-softening and Mohr–Coulomb models were adopted to simulate the mechanical behavior of the coal and roof/floor rock layers. The rock mass mechanical properties for the numerical simulation are listed in Table 4. Notably, in the strain-softening model embedded in FLAC3D, there are few guidelines for the determination of the plastic shear strain threshold. In the current study, the plastic shear strain threshold was assumed to be 0.1%. Because it is generally difficult to estimate the residual cohesion strength, the peak cohesion and friction value of the coal were scaled to the residual strength using a reduction factor of 0.1 based on past experiences in simulating coal. This factor was commonly applied for most coal measure lithologies. In the postfailure phase, the tensile strength remained unchanged based on a similar assumption in several previous studies. Table 5 presents the strain-softening parameters for the model.

In longwall mining, the roof strata of the panel cave and fall into the gob. The caved materials are compacted and consolidated afterward and thereby alter the abutment loads in the surrounding rock because a portion of the vertical

load will be supported by the consolidated materials (Wang *et al.* 2018; Yang *et al.* 2019;). Therefore, the selection of a realistic gob compaction model is an essential part of modeling the longwall mining-induced stress. Based on past experiences in simulating gob materials, in this study, the double-yield model was used to model the gob material response.

According to the available literature, the input parameters required for the double-yield Model can be divided into two groups: the cap pressure and material properties. The cap pressure could be calculated using Salamon's model, and the material properties were meticulously calibrated based on a back-analysis procedure (Wang *et al.* 2018). The final material parameters for the double-yield model are presented in Table 6.

To evaluate the reliability of the calibrated input parameters for gob modeling, the vertical stress in the gob was monitored and plotted in Fig. 7. Fig. 7 shows that the vertical stress near the coalface was approximately zero and gradually increased to 90.25% of the field stress at a distance of approximately 300 m behind the face. Previous studies reported that the vertical stress in the gob returns to the field stress at a distance of approximately 0.2-0.32 m deep below the surface. It could be concluded that the gob compaction curve is realistic because the model results of the gob model are in agreement with previous studies (Ning *et al.* 2018a).

3.2 Model validation

3.2.1 Mesh dependency

According to previous numerical simulation experience, the mesh density/size of the model has an impact on the simulation results. In this study, five models with different mesh densities/sizes were modeled to account for the mesh dependency: types I, II, III, IV and V. The five models had 720360, 991440, 1168830, 1405440, and 1649700 grid cells, respectively. Fig. 8 shows the simulated floor-to-roof convergence and rib-to-rib convergence.

Fig. 8 shows that the roadway deformation was sensitive to the mesh density of the numerical model. When the mesh density was less than 1168830, the floor-to-roof convergence and rib-to-rib convergence increased quickly. As the mesh density was increased to 1405440, the roadway deformation approached a constant level, and further increases in mesh density did not significantly improve the gateroad deformation. In other words, there was no marked difference between types V and IV, the latter of which had a smaller number of elements. This indicated that type IV is considered to be the optimum mesh density for the model configuration in view of computational efficiency.

3.2.2 Validation of the general model

The model was further validated by comparing the floor-to-roof convergence and rib-to-rid convergence observed in the field and predicted by the numerical model. One convergence station was installed during the retreat of longwall face 5305 to monitor the mining-induced floor-to-roof convergence and rib-to-rib convergence, following the monitoring methods used by Li *et al.*(2015) and Ning *et al.*(2018b) Fig. 9 displays a comparison of the tailgate deformation for the numerical model and field measurements. Fig. 9 shows that good agreement was achieved between the roadway deformation measured in the field and predicted by the numerical model. This result confirms that for this test case, the parameters used in the global model were reasonable.

4. Model results

As described in section 2.1, longwall face 5305 was divided into three regions (regions I, II and III) by the gateroad development. In the following section, the mining-induced stress changes in these three regions are discussed. During the retreat of longwall face 5305, the front abutment stress was monitored when the general model was in equilibrium. There are three ways to monitor the front abutment stress: line A, B and C. After the normal mining cycle was complete, the vertical stress in the coal seam was calculated using a FISH function and plotted in Figs. 10, 11 and 12.

To discuss the mining-induced stress changes in detail, three monitoring lines (named lines A, B and C in the following section) were set up in the numerical model when the normal mining cycle was complete. The vertical stress in the coal seam was calculated using a FISH function and plotted in Fig. 10. With the extraction of region I, along the direction of advance, the distribution of the vertical stress in the front coalface had a shape with a single peak. In region I, the stress was characterized by a stress-concentrated zone. In region II, the distribution of the vertical stress had a double peak' shape, and the peak stress occurred at the zone near the 5302 haulage roadway. After 30 m of extraction, the peak stress in the curve was approximately 2 times the premining stress. However, in region III, the curve changed to a double peak' shape. The model results indicate that in general the stress distribution caused by longwall face 5305 retreated was not similar to that caused by conventional longwall mining. This was because prior development of the roadway appeared to cut off the transfer path of the abutment stress. This cut off effect seemed to be achieved by the lack of a supporting body. The stress in this zone significantly increased due to the stress transfer. Fig. 10 shows that when the coal seam was mined for less than 30 m, the vertical stress ahead of the coalface gradually increased. However, at 40 m of face advance, yielding occurred in all areas of region I, and the stress level decreased. It can be explained that during extraction of region I, region I had an elastic core such that it supported a greater load and played an important role in the occurrence of rock burst.

The stress changes during retreat of regions II and III are plotted in Fig. 11 and Fig. 12, respectively. Fig. 11 and Fig. 12 show that ahead of the mining face, the stress concentration area occurred at the lower corner of the panel that was superimposed by three parts: the side abutment stress induced by the adjacent extraction of longwall faces 5302 and 5301; the abutment pressure induced by the advancement of longwall face 5305; and the stress induced by roadway development. The maximum vertical stress was approximately 2.2 times the original stress. It could also be

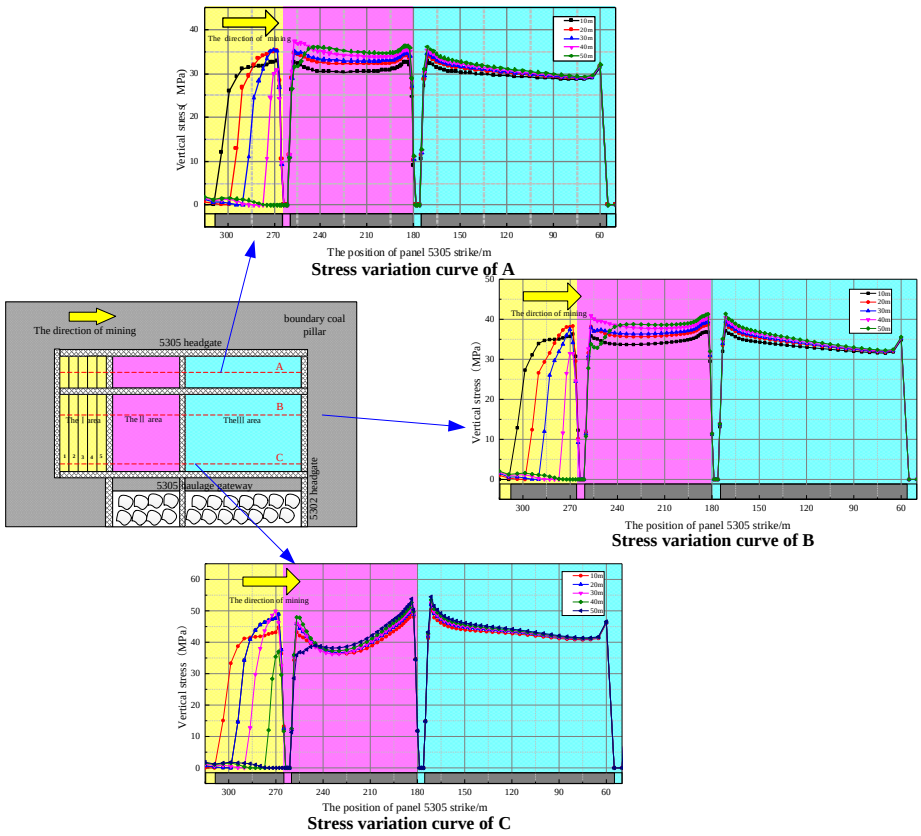

Fig. 10 Advanced vertical stress evolution map in Area I of mining panel 5305

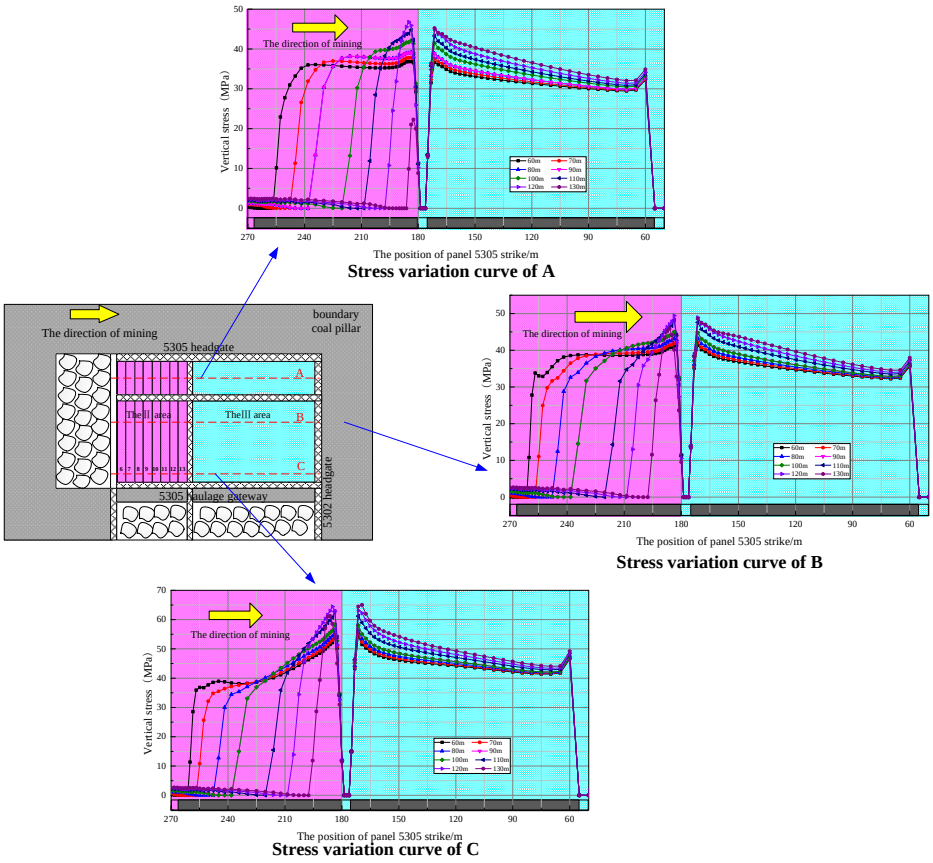

Fig. 11 Advanced vertical stress evolution map in Area II of mining panel 5305

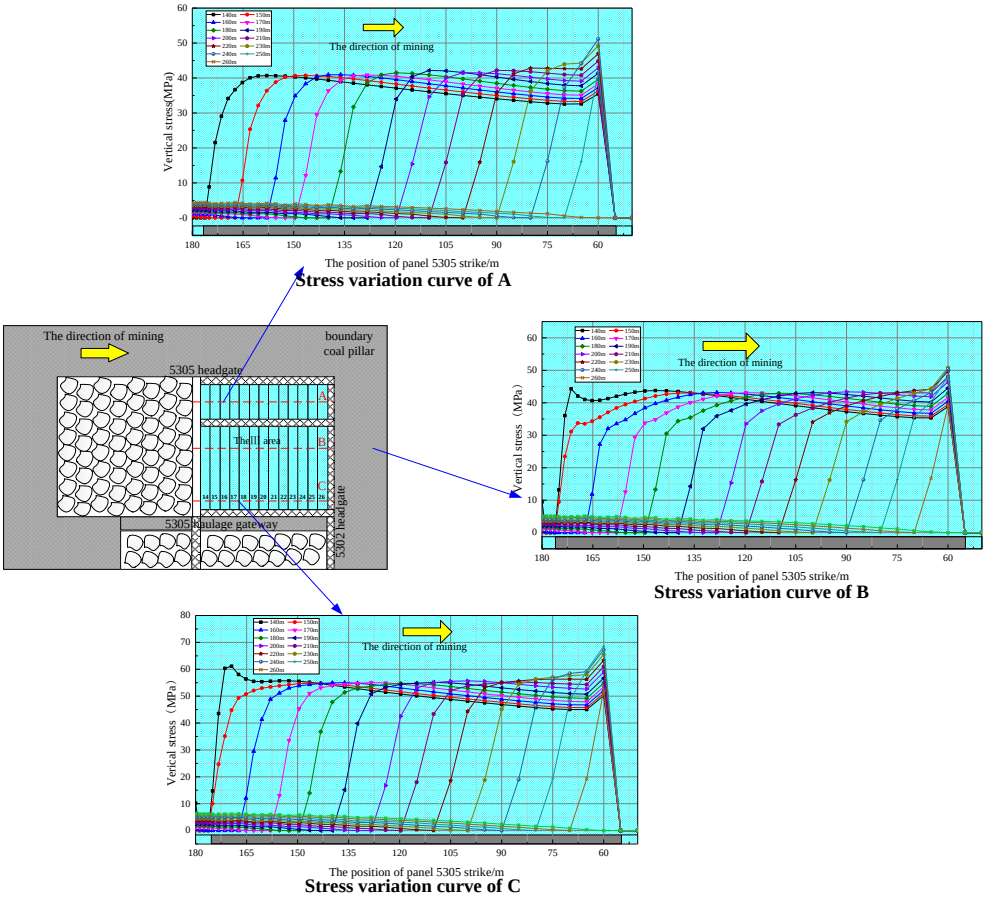

Fig. 12 Advanced vertical stress evolution map in Area III of mining panel 5305

observed that during the extraction of regions II and III, owing to the cut off effect, the distribution of the vertical stress had a similar horse-saddle shape when the width of the remaining coal seam was less than 40 m. There were two inflection points in the curve: one point occurred approximately 10 m ahead of the face, and another point occurred 13 m away from the roadway. With the continuous advance of the working face, the two inflection points merged into one point, implying that the stress superposition effect was strengthened. In this situation, the vertical stress in the final part of regions II and III increased to 2.6 times the original stress, and the peak value of the vertical stress was located at the intersection of the roadway and tailgate. This observation may explain the "6.16" and "7.24" rock burst events under high geostress.

5. Evaluation and prediction of rock burst

5.1 Impact index and testing method of the coal mass

5.1.1 Tao discriminant index (TSI)

Because rock burst can be regarded as the result of a violent tension failure in a highly stressed coal seam, it follows that the analysis of stress concentration could be used to evaluate the rock burst risk. Many stress factors have been proposed to evaluate the rock burst potential under similar stress conditions. Miao *et al.* suggested the stress factor, TSI, determined from the ratio of the intact rock strength (the uniaxial compressive strength, σ_c) to the maximum principal stress in the region of the opening Miao *et al.* (2016). Because of its simplicity, the formula is very convenient for engineering practice. It can be expressed as:

$$\mathrm{TSI}=\sigma_c/\sigma_1 \tag{1}$$

where σ_c is the uniaxial compressive strength and σ_1 is the maximum principal that can be examined with numerical simulations or field testing.

5.1.2 Brittle shear ratio index (BSR)

Canadian experience shows that microseismic events and rock bursts are dominated by crushing or shear failure under high confinement (Castro *et al.* 2012). Martin *et al.* stated that when the deviatoric stress reaches approximately 0.3-0.4 of the UCS of the rock, more microseismic events can be expected. In general, the normalized deviatoric stress is commonly used as a factor to analyze microseismic events and rock burst. According to Castro's suggestions, the brittle shear ratio (BSR) is given as:

$$\mathrm{BSR}=(\sigma_1-\sigma_3)/\sigma_c \tag{2}$$

where BSR is the brittle shear ratio.

5.1.3 Strain energy density index (SEDI)

Cook (1965) was the first to note that rock burst in deep underground mines is generally characterized by a sudden

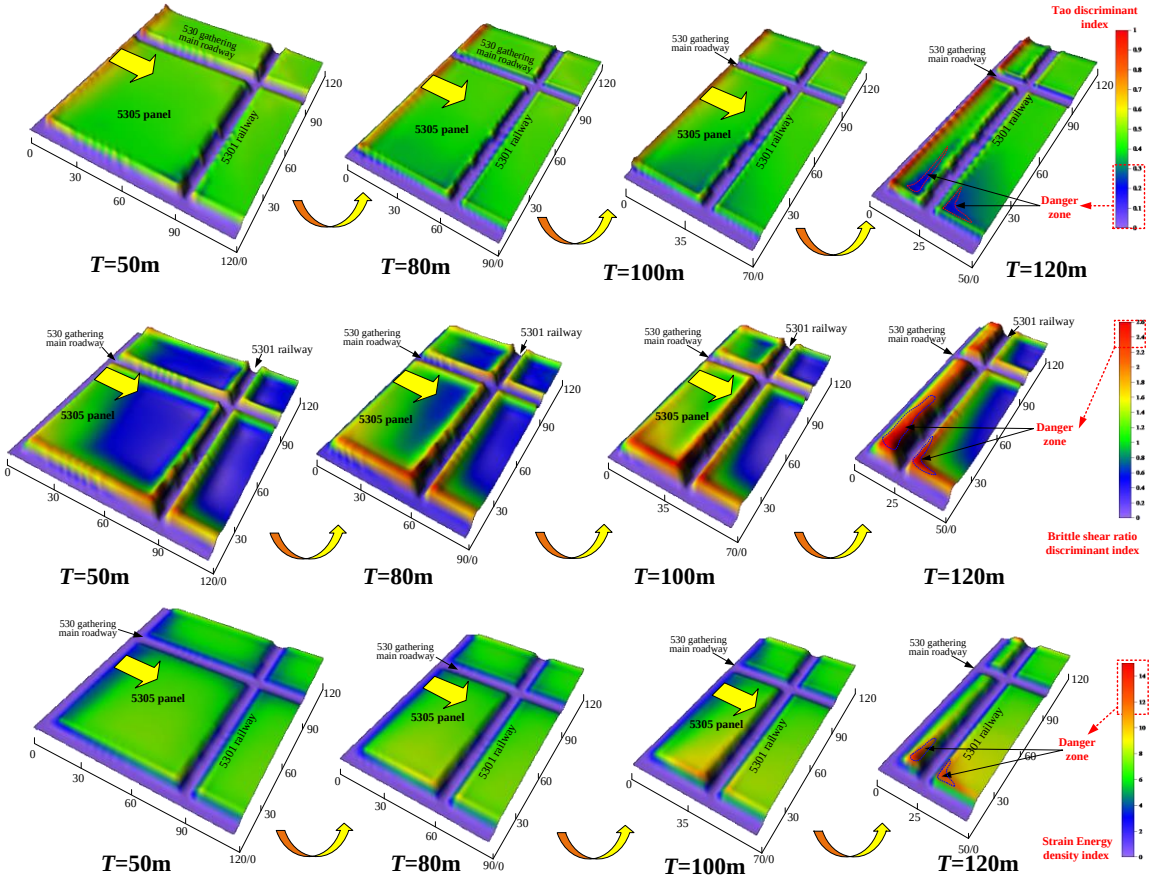

Fig. 13 Contour maps of the three indexes as the second coal pillar area is recovered

Table 7 A rock burst criterion for deep mining of the Xinhe Coal Mine

The stress and energy range	Potential for rock burst
TSI≤0.3	strong
BSR≥2.3	
SEDI≥11	

release of energy in a volume of highly stressed rock. Following Cook's contributions, several researchers investigated the link between the energy stored within rock and rock burst. Laboratory tests and theory have shown that when the energy stored within rock exceeds the limit value of the rock, some of the energy will be quickly released and may induce rock burst in the surrounding rock. The energy criterion for rock burst based on the suggestion of previous study (Chen *et al.* 2009) is expressed as follows:

$$\beta=U_d/U_0 \tag{3}$$

where U_0 is the limit value of energy that the unit volume of coal mass can store. According to studies by Cai *et al.* (2016), an assumed value of 120 kJ/m^3 can be regarded as the limit value of energy in this paper. U_d is the energy stored within the rock. The value of U_d can be estimated from the formula:

$$U_d=\left[\sigma_1^2+\sigma_2^2+\sigma_3^2-2v\left(\sigma_1\sigma_2+\sigma_2\sigma_3+\sigma_1\sigma_3\right)\right]/2E_0 \tag{4}$$

where E_0 is the loading tangential modulus and v is Poisson's ratio.

5.2 Discussion of the rock burst criteria for the Xinhe Coal Mine

In this section, the back-analyses of rock burst criteria were based on a method that utilizes the "6.16" rock burst event in combination with FLAC3D stress analysis. In sections 3 and 4, FLAC3D stress analysis was carried out to determine the principal stresses. The principal stresses were determined, and the Tao discriminant index, brittle shear ratio discriminant index and energy criterion were calculated using the FISH function embedded in FLAC3D. Fig. 13 shows the simulation results of TSI, BSR and SEDI in region II. The results in these figures show that with expansion of the stress redistribution area, the simulated α gradually decreased while BSR and SEDI increased during extraction of region II. Clearly, at 120 m of face advance, the side abutment stress, front abutment pressure and stress induced by the roadway development intersected at the intersection of the tailgate and roadway, thereby strengthening the stress superposition effect. Therefore, the largest BSR and SEDI values occurred at the intersection of the tailgate and roadway, with maximum values of approximately 2.3 and 11.0, respectively, while the smallest α also occurred at the same location, with a minimum value of approximately 0.3. After the coal seam was mined at 130 m, the coal mass in front of coalface 10 was crushed and

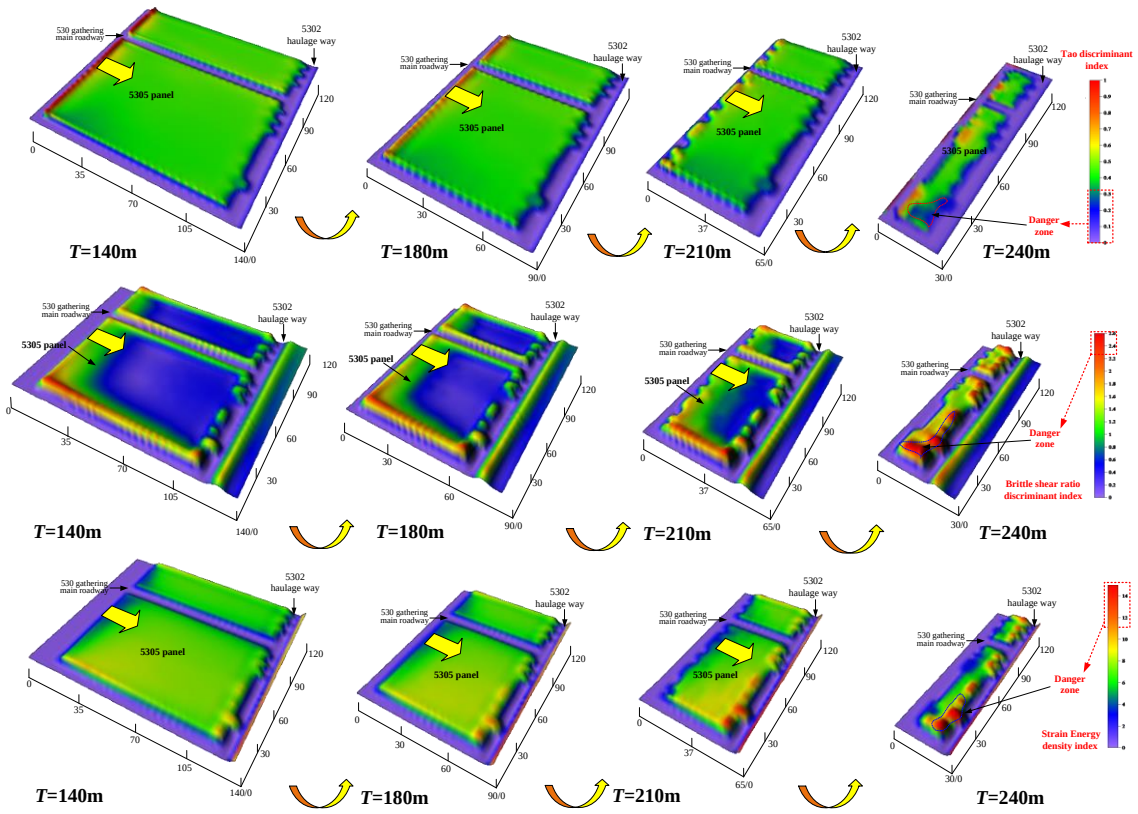

Fig. 14 Contour maps of the three indexes as the third coal pillar area is recovered

could not bear the load sufficiently. In this situation, the mining pressure was transferred to the abutment, and the stress in region II decreased. As described in section 2.4.1, the "6.16" rock burst event occurred at the same location when the longwall face advanced 126 m. The reason was that the mining-induced stress redistribution influenced the stress and energy concentration at the intersection of the tailgate and roadway. Once the stress and energy exceeded the value that the coal mass could bear, the latter led to intense seismic events and energy release, and the coal mass burst. Combined with simulation analysis, for this test case, the critical values of α, BSR and SEDI, at which it was indicated that rock burst was likely to occur, were 0.3, 2.3 and 11.0, respectively.

A great amount of theoretical analysis (Li *et al.* 2018, Hu *et al.* 2019), field investigation (Naji *et al.* 2019), and laboratory testing have shown that the burst proneness of natural coal seems to be a fundamental condition for the occurrence of rock burst in deep underground coal mines. In addition, the coal should be brittle, hard and its sudden failure is driven by a shear mechanism. Moreover, the strain energy that is stored in the coal mass should exceed the limit value that the coal mass can bear. Based on these three mechanisms, a rock burst criterion that attempts to predict the potential rock burst for deep mining of the Xinhe Coal Mine was suggested in Table 7.

5.3 Validation and discussion

5.3.1 Validation of the rock burst criteria

The suggested rock burst criteria were further validated by comparing the rock burst potential predicted by the numerical model with the field "7.24" event. Laboratory tested results showed that the coal mass in region III also exhibited susceptibility to bursting. Then, in the following section, both the stress and energy indicators were validated. Fig. 14 shows the simulated TSI, BSR and SEDI results during the excavation of region III.

As shown in Fig. 14, it can be observed that before region III was mined at 90 m, the values of TSI, BSR and SEDI followed: $0.33<TSI<1.0$, $0<BSR<2.1$ and $0<SEDI<10.2$. According to the suggested rock burst criteria, the model results indicated that rock burst potential was not present in region III, which was in agreement with field observations. However, at 100 m of excavation of region III, TSI, BSR and SEDI reached 0.28, 2.41 and 12.2, respectively. The value of these three indicators met the suggested rock burst criteria, implying that there was rock burst potential at the intersection of the tailgate and roadway. Field observation showed that the "7.24" rock burst event also occurred at the same location. It could be concluded that the suggested rock burst criteria are reasonable because the rock burst potential predicted by the numerical model is in agreement with field observations.

5.3.2 Discussion

The proposed rock burst criteria indicated that when $TSI<0.3$ rock burst could occur. The suggested critical value of TSI is not in agreement with previous studies. Miao *et al.* (2016) proposed $TSI\leq2.5$ for hard and brittle rock [15]. In

underground coal mines, the coal mass has relatively weak properties compared to Lac du Bonnet granite, which has a uniaxial compressive strength (UCS) of 150-300 MPa. However, most coal seams have a UCS less than 35 MPa. Thus, it can be expected that the weak properties of coal contribute to the difference between the suggested critical value and previous studies. In addition, in this study, the suggested critical value of BSR was 2.3, which is greater compared to other study results. In deep underground coal mines, the surrounding rock is subjected to high vertical stresses (at a ratio of vertical-to-horizontal stress of approximately 2-3), which is approximately 3-4 times the UCS of coal. In this situation, BSR was likely to be different from that of hard rock. Considering this difference, the suggested critical values of TSI and BSR may be considered as being representative of coal failure. Similarly, the criterion value of SEDI is different from that of Miao *et al.* (2016) due to the difference in the storage characteristics of the 5305 plane, and thus, the elastic strain energy threshold obtained by field verification should agree with the actual situation of the Xinhe Coal Mine.

The prediction of rock burst in deep coal seam mining is the foundation for protection against and prevention of rock burst damage. This paper aimed to establish criteria based on back-analysis. The suggested rock burst criteria are characterized by combining the burst proneness, stress and several energy indicators of coal. In conjunction with numerical analysis (i.e., FEM or DEM models) of the stress or energy distribution, the coal mass with a high rock burst risk can be mapped. Therefore, timely active measures to lower the rock burst potential should be taken. However, it should be mentioned that the rock burst criteria only delineate the danger zone, but could not determine the magnitude of rock burst. Therefore, determining the classification criteria of the rock burst magnitude will be carried out in future work, combined with analysis of a large number of rock burst cases.

6. Conclusions

Based on the typical geological settings in the Xinhe Coal Mine, a simplified numerical model of panel 5305 was constructed with the finite difference code FLAC3D. Back-analyses of rock burst criteria were based on methods that utilized field rock burst events in combination with FLAC3D stress analysis results. The main conclusions drawn from the study can be summarized as follows:

(1) The most notable characteristic of the advance abutment pressure was that the transfer path was cut off by prior development of the roadway. In the early stage of mining, the advance abutment pressure of the pillar area between two adjacent parallel roadways presented a horse-saddle shape, and two peaks appeared. With the advance of the working face, the two peaks gradually converged to form a single peak. At the end of regional pillar mining, the advance abutment pressure transferred to the next pillar within a shorter advancing distance, which made rock burst events likely to occur.

(2) Based on the combination of field rock burst events and FLAC3D analysis results, rock burst criteria for the Xinhe Coal Mine were established by back-analysis. In the mining process, the Tao discriminant index, brittle shear ratio discriminant index and strain energy density index in part of the advancing working face reached TSI<0.3, BSR>2.3 and SEDI>11, and the area was considered to be at risk of strong shocks. Based on the "7.24" rock burst event, reasonable rock burst criteria were proposed.

(3) In the process of estimating the local stability of deep mining, a semiquantitative method was adopted. The research results are preliminary and need to be further revised and deepened by practical application under specific engineering conditions.

Acknowledgments

The research described in this paper was financially supported by National Key R&D Program of China (No. 2018YFC0604703); National Natural Science Foundation of China (No. 51574154, 51804181); Major Program of Shandong Province Natural Science Foundation (no. ZR2018ZA0603); Key R & D programs of Shandong Province (no. 2018GSF116003); Shandong Province Natural Science Fund (no. ZR2018QEE002, ZR2017BEE013). SDUST Graduate Student Technology Innovation Project (No. SDKDYC190116) The authors express sincere thanks to the reviewers for their helpful comments and suggestions for improving this paper.

References

Brady, B.H.G. and Brown, E.B. (2006), *Rock Mechanics for Underground Mining*, Springer, The Netherlands.

Cai, M.F. (2016), "Prediction and prevention of rock burst in metal mines–a case study of Sanshandao gold mine", *J. Rock Mech. Geotech. Eng.*, **8**(2), 204-211. https://doi.org/10.1016/j.jrmge.2015.11.002.

Castro, L.A.M., Bewick, R.P. and Carter, T.G. (2012), *An Overview of Numerical Modelling Applied to Deep Mining*, in *Innovative Numerical Modelling in Geomechanics*, CRC Press, London, U.K., 393-414.

Chen, W.Z., Lu, S.P. and Guo, X.H. (2009), "Research on unloading confining pressure tests and rockburst criterion based on energy theory", *Chin. J. Rock Mech. Eng.*, **28**(8), 1530-1540.

Cook, N.G.W. (1965), "The failure of rock", *Int. J. Rock Mech. Min. Sci. Geomech. Abstr.*, **2**, 389-403. https://doi.org/10.1016/0148-9062(65)90004-5.

Fan, D.Y., Liu, X.S., Tan, Y.L, Yan, L. Song, S.L. and Ning, J.G. (2019), "An innovative approach for gob-side entry retaining in deep coal mines: A case study", *Energy Sci. Eng.*, 1-15. https://doi.org/10.1002/ese3.431.

GB/T 25217.2-2010 (2010), "Classification and laboratory test method on bursting liability", *Coal Standards Press of China*, Beijing, China.

Hoek, E. and Marinos, P.G. (2010), "Tunnelling in overstressed rocks. Rock engineering in difficult ground conditions—soft rocks and karst", *Proceedings of the Regional Symposium of the International Society for Rock Mechanics, EUROCK 2009*, Dubrovnik, Croatia, October.

Hu, S.C., Tan, Y.L., Zhou, H., Ru, W.K., Ning, J.G., Wang, J., Huang, D.M. and Li, Z. (2019), "Anisotropic modeling of layered rocks incorporating planes of weakness and volumetric stress", *Energy Sci. Eng.*, https://doi.org/10.1002/ese3.551.

Li, W.F., Bai, J.B., Syd, P., Wang, X.Y. and Xu Y. (2015), "Numerical modeling for yield pillar design: A case study", *Rock Mech. Rock Eng.*, **48**(1), 305-318. https://doi.org/10.1007/s00603-013-0539-8.

Li, Z., Zhou, H., Jiang, Y., Hu, D.W. and Zhang, C.Q. (2018), "Methodology for establishing comprehensive stress paths in rocks during hollow cylinder testing", *Rock Mech. Rock Eng.*, **52**(4), 1055-1074. https://doi.org/10.1007/s00603-018-1628-5.

Liu, W.T., Zhao, J.Y., Nie, R., Zeng, Y., Xu, B. and Sun, X. (2019), "A full coupled thermal-hydraulic-chemical model for heterogeneity rock damage and its application in predicting water inrush", *Appl. Sci.*, **9**, 2195. https://doi.org/10.3390/app9112195.

Liu, X.S., Gu, Q.H., Tan, Y.L., Ning, J.G. and Jia, Z.C. (2019), "Mechanical characteristics and failure prediction of cement mortar with a sandwich structure", *Minerals*, **9**(3), 143. https://doi.org/10.3390/min9030143.

Liu, X.S., Tan, Y.L., Ning, J.G., Lu, Y. and Gu, Q.H. (2018), "Mechanical properties and damage constitutive model of coal in coal-rock combined body", *Int. J. Rock Mech. Min. Sci.*, **110**, 140-150. https://doi.org/10.1016/j.ijrmms.2018.07.020.

Mazaira, A. and Konicek, P. (2015), "Intense rock burst impacts in deep underground construction and their prevention", *Can. Geotech. J.*, **52**(10), 1426-1439. https://doi.org/10.1139/cgj-2014-0359.

Miao, S.J., Cai, M.F., Guo, Q.F. and Huang, Z.J. (2016), "Rock burst prediction based on in-situ stress and energy accumulation theory", *Int. J. Rock Mech. Min. Sci.*, **83**, 86-94. http://dx.doi.org/10.1016%2Fj.ijrmms.2016.01.001.

Mitri, H.S. (1999), "FE modelling of mining-induced energy release and storage rates", *J. S. Afr. Inst. Min. Metall.*, **99**(2), 103-110.

Naji, A.M., Emad, M.Z., Rehman, H. and Yoo, H. (2019), "Geological and geomechanical heterogeneity in deep hydropower tunnels: A rock burst failure case study", *Tunn. Undergr. Sp. Technol.*, **84**, 507-521. https://doi.org/10.1016/j.tust.2018.11.009.

Ning, J.G., Liu, X.S., Tan, J., Gu, Q.H., Tan, Y.L. and Wang, J. (2018a), "Control mechanisms and design for a 'col-backfill-gangue' support system for coal mine gob-side entry retaining", *Int. J. Oil Gas Coal Technol.*, **18**(3-4), 444-465.

Ning, J.G., Wang, J., Jiang, J.Q., Hu, S.C., Jiang, L.S. and Liu, X.S. (2018b), "Estimation of crack initiation and propagation thresholds of confined brittle coal specimens based on energy dissipation theory", *Rock Mech. Rock Eng.*, **51**, 119-134. https://doi.org/10.1007/s00603-017-1317-9.

Shang, H.F., Ning, J.G., Hu, S.C., Yang, S. and Qiu, P.Q. (2019), "Field and numerical investigations of gateroad system failure under an irregular residual coal pillar in close-distance coal seams", *Energy Sci. Eng.*, 1-21. https://doi.org/10.1002/ese3.455.

Wang, J., Ning, J.G., Jiang, L.S., Jiang, J.Q. and Bu, T.T. (2018a), "Structural characteristics of strata overlying of a fully mechanized longwall face: a case study", *J. S. Afr. Inst. Min. Metall.*, **118**, 1195-1204. http://dx.doi.org/10.17159/2411-9717/2018/v118n11a10.

Wang, J., Ning, J.G., Qiu, P.Q., Yang, S. and Shang, H.F. (2018b), "Microseismic monitoring and its precursory parameter of hard roof collapse in longwall faces: A case study", *Geomech. Eng.*, **17**(4), 375-383. https://doi.org/10.12989/gae.2019.17.4.000.

Yang, S., Wang, J., Li, X.H., Ning, J.G. and Qiu, P.Q. (2019), "In situ investigations into mining-induced hard main roof fracture in longwall mining: A case study", *Eng. Fail. Anal.*, **106**, 104188. https://doi.org/10.1016/j.engfailanal.2019.104188.

Zhao, T.B., Guo, W.Y., Tan, Y.L., Lu, C.P. and Wang, C.W. (2018), "Case histories of rock bursts under complicated geological conditions", *Bull. Eng. Geol. Environ.*, **77**, 1529-1545. https://doi.org/10.1007/s10064-017-1014-7.

Zhu, S.T., Feng, Y., Jiang, F.X. and Liu, J.H. (2018), "Mechanism and risk assessment of overall-instability-induced rockbursts in deep island longwall panels", *Int. J. Rock Mech. Min. Sci.*, **106**, 342-349. https://doi.org/10.1016/j.ijrmms.2018.04.031.

CC